Mechanical characterization of solution-derived nanoparticle silver ink thin films

Julia R. Greer[a] and Robert A. Street
Palo Alto Research Center (PARC), 3333 Coyote Hill Road, Palo Alto, California 94304

(Received 22 January 2007; accepted 23 March 2007; published online 29 May 2007)

Mechanical properties of sintered silver nanoparticles are investigated via substrate curvature and nanoindentation methods. Substrate curvature measurements reveal that permanent microstructural changes occur during initial heating while subsequent annealing results in nearly elastic behavior of the thinner films. Thicker films were found to crack upon thermal treatment. The coefficient of thermal expansion was determined from linear slopes of curvature curves to be 1.9 ± 0.097 ppm/°C, with elastic modulus and hardness determined via nanoindentation. Accounting for substrate effects, nanoindentation hardness and modulus remained constant for different film thicknesses and did not appear to be a function of annealing conditions. Hardness of 0.91 GPa and modulus of 110 GPa are somewhat lower than expected for a continuous nanocrystalline silver film, most likely due to porosity. © *2007 American Institute of Physics*. [DOI: 10.1063/1.2735404]

I. INTRODUCTION

Nanoparticle metal inks present a promising candidate for large-area electronics applications as they are compatible with jet printing and low-temperature processing conditions required by flexible substrates. Usually, a thermal cure is required subsequent to the solution-based deposition to achieve the ink's transformation into the solid phase. For these applications it is important to understand the mechanical behavior of these materials, specifically the stress development as a function of various thermal cure processes. The specific silver nanoink used in this work consists of ~40 nm silver particles with ~5 nm polymer shell suspended in ethylene glycol. A unique feature of the nanoink-derived features is that they are formed from a room-temperature solution either jet printed or spin coated on a substrate. When the ink is subjected to various thermal annealing conditions, the silver nanoparticles begin to sinter at temperatures slightly above 100 °C due to their high surface area-to-volume ratio,[1] inducing mechanical stress in the film and in the substrate. These mechanical stresses arise mainly from the evaporation of the solvent as well as from the difference in thermal expansion coefficients between the Si substrate and the forming silver films. Wafer curvature measurements can provide important information about the film's elastic and plastic properties when either the coefficient of thermal expansion or the biaxial modulus is known.[2] Determination of these parameters for nanoinks has to be done empirically rather than inferred from literature.

II. MECHANICAL STRESSES IN THIN FILMS: CURVATURE MEASUREMENTS

To determine the residual stresses, films of several thicknesses were heated to 150 °C at a constant rate of ~3 °C/min, held isothermally for 1 h, and then cooled at the same rate. Film thickness variation was achieved by varying the spin-coating speed between 800 and 2500 rpm and thermal treatment conditions, resulting in thicknesses between 650 and 110 nm, respectively. The radius of curvature, R, was monitored throughout each test in a Tencor FLX-2320 thin film stress measurement system and related to the film stress by the Stoney relation[3]

$$\sigma_f = \left(\frac{E_s}{1-\nu_s}\right)\frac{t_s^2}{6t_f}\left(\frac{1}{R}-\frac{1}{R_0}\right). \quad (1)$$

The thin film approximation is applicable here since the Si substrate is much thicker than the film, and hence, the residual film stress depends only on the elastic properties of the substrate and is independent of the film properties. In a typical wafer curvature experiment, the film thickness remains constant throughout the annealing, and the film stress is determined from the radius of curvature automatically by the Tencor software using Eq. (1). In this case, however, even after the solvent vaporizes, the film thickness continues to decrease throughout the cure process due to densification induced by sintering. The amount of linear shrinkage in these films was monitored and measured via a Dektak profilometer throughout the thermal cure and stresses were calculated according to Eq. (1) with the appropriate film thickness. A detailed description of nanosilver film thickness variation with thermal cure doncitions is discussed by the authors elsewhere.

A representative stress-temperature behavior during two consecutive heatings to 150 °C and cooling to room temperature cycles of a 200-nm nanoink film is shown in Fig. 1. The first heating of the ink up to 85 °C does not induce any film stress until the solvent evaporates and a solid film forms. Therefore, the initial heating region in Fig. 1 is characterized by an essentially stress-free state until ~85 °C. A significant jump in stress up to ~35 MPa is observed between 95 and 100 °C when sintering begins, suggesting a higher rate of thickness loss. Between the point of solvent evaporation and 150 °C the film continuously loses ~13% of its initial thickness.[4] Subsequently, the film stress gradually increases

[a]Electronic mail: jrosolov@alum.mit.edu

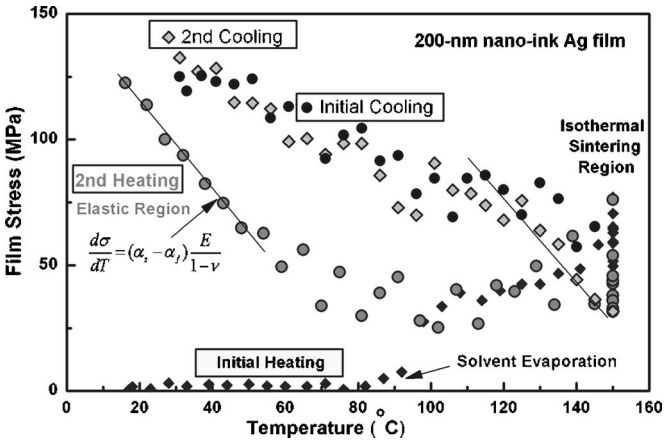

FIG. 1. Stress as a function of temperature as determined by wafer curvature measurements. During initial hearing, solvent evaporation is followed by the sintering region characterized by a significant increase in the stress. During the subsequent cycle initial deformation on heating is elastic as indicated by the linear slope line.

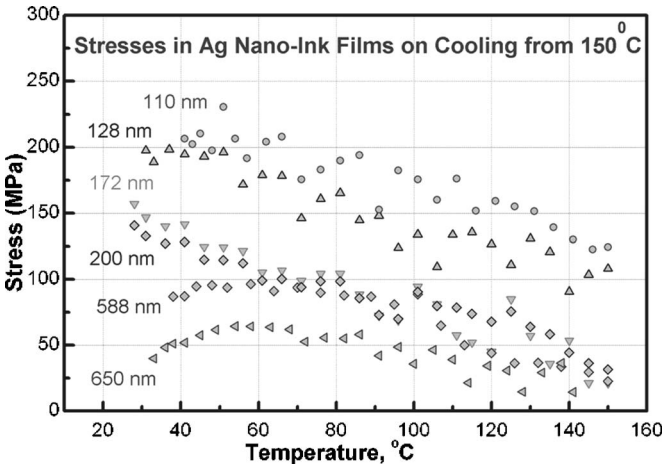

FIG. 2. Stress development upon cooling for film thicknesses between 110 and 650 nm. Thinner films exhibit initial linear elasticity followed by yielding while the two thicker films demonstrate a plateau followed by relaxation.

up to 60 MPa at 150 °C and remains virtually unchanged throughout the isothermal anneal. The final film thickness is achieved during this anneal and remains relatively unchanged upon further thermal fluctuations. During this time, the microstructure of the film changes as it densifies by sintering. Upon cooling, tensile stress continues to build up in the film due to the higher coefficient of thermal expansion (CTE) in the film compared with the Si substrate. Subsequent thermal cycling shows a reproducible typical elastic-plastic hysteresis loop indicating that the metal film has become mechanically stable. In the initial stages of the second heating (cooling) regions, the reduction (increase) of tensile stress in the film is due to the mismatch in the CTEs between the film and the substrate and in this regime the stress is linearly proportional to the strain through the biaxial elastic modulus. Thermal expansion coefficient can, therefore, be determined from the slope of this elastic second heating curve using the elastic modulus

$$\frac{d\sigma}{dT} = (\alpha_s - \alpha_f)\frac{E}{1-\nu}, \tag{2}$$

where α_s and α_f are CTEs of the substrate and the film, respectively, and $E/1-\nu$ is the biaxial modulus. The elastic modulus is obtained via nanoindentation as described in the following section.[5] An interesting feature of the second heating section in Fig. 1 is that the stress in the film remains nearly constant between 80 and 150 °C. Normally, this region would be characterized by a compressive plastic flow in the film driven by higher thermal expansion of the film relative to the Si substrate. In the case of this nanoink-derived film, its overall stress response is clearly tensile, between 25 and 50 MPa. This behavior might be attributed to the inhomogeneous stress distribution throughout the film thickness. In this case, the bottom-most layer would experience compression due to the CTE mismatch, as expected, while the top-most regions might remain in tension, driving the overall stress state of the film to be slightly tensile. Factors like incomplete solvent evaporation and competing sintering/diffusion mechanisms are expected to contribute to the creation of this inhomogeneous-stress distribution. This effect is further exacerbated by the lack of tight distribution in the curvature data. The wide spread in the radius of curvature data, and hence, in the stress data, is also attributed to long measurement times, during which the temperature was continuously increased rather than held constant, and to the film surface roughness affecting the laser beam reflection.

Residual tensile stresses developed in the nanoparticle metal films of different thicknesses upon cooling from 150 °C down to the room temperature were below ~225 MPa, as can be seen in Fig. 2. The highest tension of 220 MPa was achieved by the thinnest, 110 nm film, and the residual tensile stresses decreased with the increasing film thickness. An interesting aspect of this plot is that while above 80 °C the deformation is mainly elastic for all films, the subsequent mechanical response is different for thinner films compared with the thicker ones. In the 110, 128, 172, and 200 nm films, the stress continues to gradually rise at the same rate, while for thicker films (588 and 650 nm), the region between 85 and 50 °C is characterized by a plateau in stress. Furthermore, these films exhibit partial relaxation as the cooling curve tends toward 0 past ~50 °C.

III. CHARACTERIZATION OF MICROSTRUCTURE

The observed stress relaxation is apparently due to cracking. Thicker films (450 nm and above) consistently cracked after thermal treatment, with typical tensile fracture patterns on the surface, as can be seen in the microscope image in Fig. 3. No crack formation was observed for thinner films. The cracks in thicker films are initiated at a flaw inside the film, and subsequent propagation is driven by the elastic strain energy stored in the film under biaxial tensile stress. The initial small cracks will only grow if the energy stored in a film is greater than that required for fracture, with the critical thickness for fracture being inversely proportional to the square of the film stress[6]

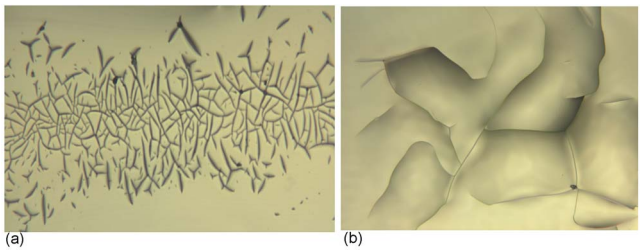

FIG. 3. Optical microscope images of cracking in 650-nm nanoink films cured at 150 °C and cooled off to the room tempearture. (a) 5× magnification of the center region. (b) 20× magnification.

$$h_f = \frac{G_{\text{steady}} E_f}{Z\sigma_f^2}, \tag{3}$$

where G_{steady} is the driving force for fracture, σ_f is the film stress, E_f is the elastic modulus, and Z is a dimensionless factor specific to different crack shapes.[7–9] The subscript "steady" here implies that once the crack length exceeds the film thickness, as it does in this case, crack propagation occurs at a steady state and is independent of the initial flaw size.[10] By using the appropriate Z value of 1.98 and estimating $G \sim 10$ N/m, we found that these nanoink films cracked below their estimated critical thickness of ~ 8 μm. This is most likely due to the nature of solid film formation from the liquid phase into a solid one via solvent diffusion and evaporation. These processes can result in an inhomogeneous stress distribution throughout the film thickness, with much higher tensile stresses developed in the top-most surface layer compared with the bottom layer, which can exacerbate crack formation. While the initial cooling region in the stress-temperature plots is characterized by a linear elastic response in films of all thicknesses, thicker films undergo a partial relaxation during intermediate cooling region (temperatures between 80 and 50 °C), as the more stressed localized regions relax at the expense of the less stressed segments. The overall film stress, therefore, remains unchanged, as indicated by the plateau region. Upon further cooling, the tensile stress builds up further, and once it exceeds the material's fracture strength in the top-most layer, the strain energy is relieved through cracking. Cracking is not observed in thinner films, where solvent diffusion is limited to a much smaller amount of material, and the strain energy can be accommodated through a higher homogeneous tensile stress developed in the film.

Despite this pronounced difference in mechanical behavior upon cooling, the microstructure of all films was identical. Typically, the grain sizes in annealed polycrystalline films are on the order of 3× the film thickness;[11] the microstructure here, however, consists of a network of sintered particles, slightly larger than their initial size, and does not vary with the film thickness. In all films, the grain size remained the same, on the order of 50 nm, and the grains appeared to be stacked vertically throughout the film height, as shown by the cross-sectional scanning electron microscopy (SEM) image in Fig. 4. The last image in the figure shows a zoomed-in crack region, clearly showing the interparticle rather than intraparticle segregation.

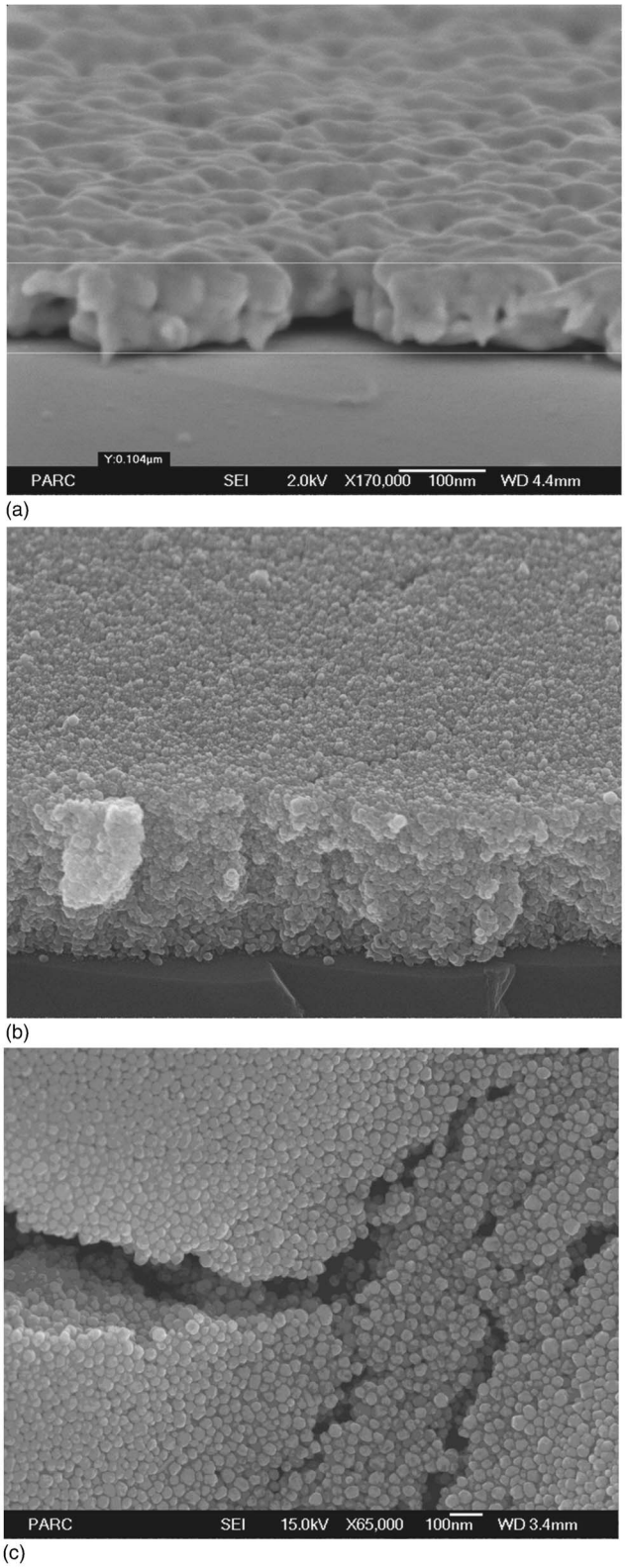

FIG. 4. SEM images of (a) 3-h-120 °C-cured film (cross section). The sintered grains are clearly stacked upon each other throughout the film thickness. (b) 500-nm film after 5-min 150 °C cure showing no cracks (cross section). (c) Zoomed-in crack region for the 600-nm samples after solvent evaporation (top view).

IV. NANOINDENTATION ANALYSIS

We determined the elastic modulus of these nanoink derived silver films by nanoindentation. This technique is very

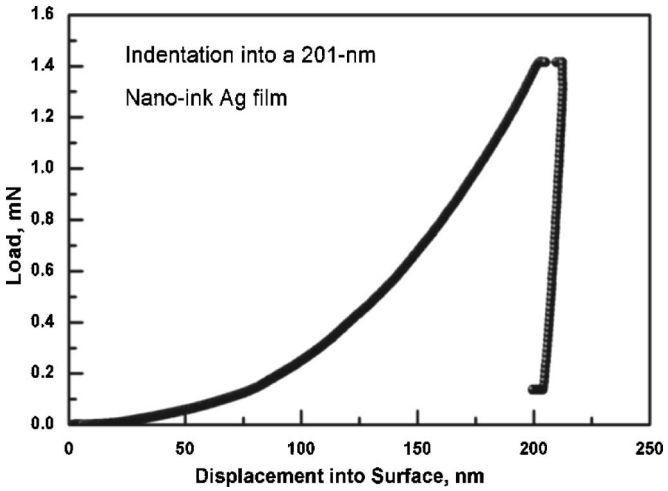

FIG. 5. Nanoindentation load-displacement curve for 201-nm nanoink silver film on a Si substrate.

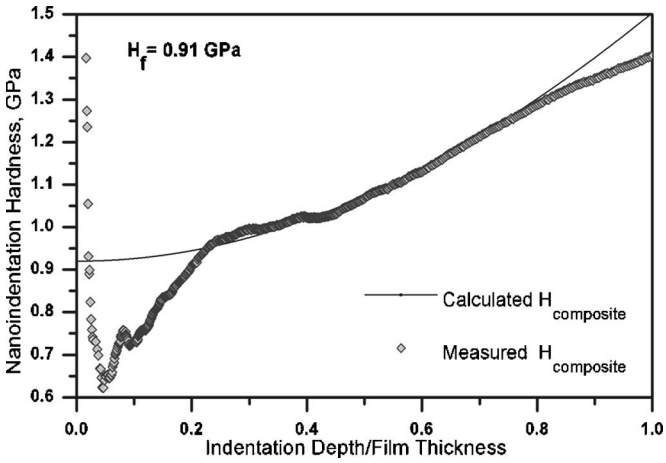

FIG. 6. Indentation hardness as a function of fractional indentation depth: experimental data (open diamonds) and calculated composite hardness based on Eq. (7). Resulting film hardness of 0.91 GPa is shown in the top left corner.

effective for studying mechanical properties of thin films as it induces localized mechanical deformation while measuring load and displacement with very high resolution.[12] All nanoindentation experiments were performed in the MTS Nanoindenter XP, which operates by loading a sharp diamond indenter tip into the sample while measuring its displacement into surface. A typical load-displacement curve obtained for the Ag nanoink films is shown in Fig. 5. Elastic modulus, E, and hardness, H, which is proportional to its yield strength, represent the typical properties inferred from nanoindentation experiments.[13] Our experiments were run in a continuous stiffness measurement mode, which enabled a precise determination of the stiffness though a dynamic response. Specifically, the Oliver–Pharr analysis method was used to determine the modulus at each indentation depth as a function of stiffness, S, and contact area, A_c,

$$S = E^* \frac{\sqrt{\pi}}{2\beta\sqrt{A_c}}, \tag{4}$$

where β is a geometric constant of 1.034 for pyramidal indenters[14] and E^* is the reduced elastic modulus of the film/indenter system represented by the following equation:

$$E^* = \left(\frac{1-\nu_{\text{film}}}{E_{\text{film}}} + \frac{1-\nu_{\text{indenter}}}{E_{\text{indenter}}} \right)^{-1}. \tag{5}$$

The contact area is a polynomial function of the contact depth whose coefficients are unique for each indenter shape and are determined prior to the indentation experiments.

The composite film-substrate hardness was determined at each indentation depth by dividing the instantaneous applied load, P, by the contact area, A_c,[12]

$$H = \frac{P}{A_c} = \frac{P(h_c)}{24.5h_c^2 + C(h_c)}. \tag{6}$$

To examine the effects of film thickness on modulus and hardness, four different film thicknesses were investigated. After solvent evaporation, the samples were subjected to isothermal cure at different temperatures: 120, 150 (two samples), and 180 °C. The cure times were chosen such that the electrical resistivity reached 50% of its initial value, i.e., 3 h for 120 °C, 30 min for 150 °C, and 10 min for 180 °C. The dependence of resistivity and final film thickness on isothermal cure times and temperatures is discussed elsewhere.[4] This combination of spin-coating speed and thermal annealing conditions resulted in the film thicknesses of 104, 201, 234, and 304 nm.

The depth of nanoindentation is one of the key considerations for obtaining true mechanical properties of a film-on-a-substrate system. When the indentation depth becomes on the order of 10% of the film thickness, substrate effects start playing an important role in the determination of hardness and modulus.[15,16] On the other hand, at indentation depths less than the surface roughness, the contact area is not well defined, which prevents precise calculation of the hardness. Atomic force microscopy results indicate that the surface roughness of the nanoink films is on the order of 40 nm. In order to account for the substrate effects, we use the methodology developed by Korsunsky *et al.*,[17] which allows for the calculation of the true film hardness from that measured on a film-on-a-substrate system

$$H_{\text{meas}} = H_{Si} + \frac{H_f - H_{Si}}{1 + h^2/\chi t}, \tag{7}$$

where H represents the respective hardness, h is the indentation depth, and χ is a geometric parameter. Since the film thicknesses discussed here were less than 400 nm, as is typical of printed features, the hardness and modulus of each sample were obtained by averaging the results of eight indentations between displacements of 40 and 100 nm and by applying Eq. (7). H_s of 10.5 GPa was used in fitting the experimental hardness versus indentation depth curves and χ varied between 3×10^{-6} for the 104 nm film and 2.3×10^{-6} for the 304 nm film.

An example of the composite (film+substrate) hardness variation calculated based on Eq. (7) as compared with our data is shown as a function of indentation depth/film thickness in Fig. 6. The graph shows a monotonic increase in hardness as the indentation becomes deeper. A good agree-

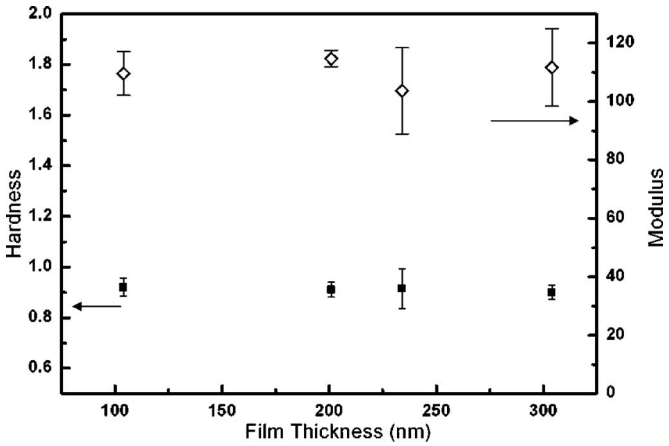

FIG. 7. Hardness (filled squares) and biaxial modulus (open diamonds) vs film thickness. Both parameters remain independent of film thickness.

ment between the experimental and calculated curves is observed for fractional indentation depths between 0.25 and 0.75. We inferred the film hardness by averaging experimental values over fractional indentation depths between 0.3 and 0.5. The modulus was calculated using Eq. (4) from the instantaneous stiffness and contact area. Figure 7 shows that both hardness (open symbols) and biaxial modulus (filled symbols) are independent of film thickness and cure conditions, as they remain within the standard deviation for all four samples. Using this technique to determine hardness of thin Ag films sputtered at room temperature, Panin *et al.*[15] found the true film hardnesses to be 1.5 GPa for 100-nm-grained and 0.7 GPa for 400-nm-grained film, suggesting that the hardness increases with decreasing grain size. Extensive work on understanding the mechanical properties of polycrystalline thin films also indicates that the flow stress, and therefore hardness, decreases with increasing grain size.[18–21] Therefore, for 50-nm-grained films, the expected hardness would be on the order of 1.8 GPa. In our films, however, the average hardness was ~0.91 GPa, approximately equal to half of the hardness of an equivalent-grain-size nanocrystalline silver films. The average elastic modulus of 110 GPa also did not appear to be affected by the film thickness and is somewhat lower than modulus of 148 GPa reported by Panin *et al.*[15] The lower values of both elastic modulus and hardness can be explained by the incomplete sintering of the film, remaining porous after thermal treatment. Greer *et al.*[4] determined the relationship between linear shrinkage of the nanoink Ag films and thermal cure. Based on their work, the resulting film thicknesses of the films subjected to the specific treatment conditions used here should be between 85% and 88% of their initial solid thickness. The presence of pores, or air pockets between some of the grains, leads to a reduction in elastic and plastic properties of the material.

The elastic modulus determined by nanoindentation was used to calculate the film's CTE from the slope of the second heating curve in Fig. 1 and Eq. (2) and turned out to be 1.9 ± 0.097 ppm/°C. This agrees very well with the literature value of 1.91 ppm/°C for pure Ag.[6] It is reasonable that the CTE remains the same and is not affected by the pores.

V. CONCLUSIONS

In summary, we investigated mechanical behavior of solution-processed nanoink silver films of various thicknesses subjected to different thermal treatment conditions. We found that films thicker than ~450 nm cracked most likely due to the inhomogeneous stress distribution throughout the film thickness. Thinner nanoink films appeared to behave similarly to their sputter-deposited counterparts although with somewhat degraded mechanical properties. A combination of nanoindentation and wafer curvature measurements allowed for determination of the biaxial elastic modulus (110 GPa), indentation hardness (910 MPa), and the coefficient of thermal expansion (1.91 ppm/°C). While the CTE agrees well with that of the bulk silver, both modulus and hardness are ~20% lower than the sputtered films of similar thicknesses, most likely due to the residual porosity in the films.

ACKNOWLEDGMENTS

The authors gratefully acknowledge Fred Endicott for SEM support and Cabot Corporation for providing the inks.

[1] Ph. Buffat and J.-P. Borel, Phys. Rev. A **13**, 2287 (1976).
[2] S. Gardner and P. Flinn, IEEE Trans. Electron Devices **35**, 2160 (1988).
[3] G. G. Stoney, Proc. R. Soc. London, Ser. A **82**, 172 (1909).
[4] J. R.Greer and R. A. Street, Acta Mat. (2007) (submitted).
[5] J.-H. Zhao, T. Ryan, P. S. Ho, A. J. MkKerrow, and W.-Y. Shih, J. Appl. Phys. **85**, 6421 (1999).
[6] L. B. Freund and S. Suresh, *Thin Film Materials* (Cambridge University Press, Cambridge, 2003), p. 286.
[7] J. W. Hutchinson and Z. Suo, Adv. Appl. Mech. **29**, 63 (1992).
[8] R. Huang, J. H. Prevost, Z. Y. Huang, and Z. Suo, Eng. Fract. Mech. **70**, 2513 (2003).
[9] J. J. Vlassak, Y. Lin, and T. Y. Tsui, Mater. Sci. Eng., A **391**, 159 (2005).
[10] Z. Suo, J. Vlassak, and S. Wagner, China Particuol. **3**, 321 (2005).
[11] C. V. Thompson, Annu. Rev. Mater. Sci. **20**, 245 (1990).
[12] W. Oliver and G. Pharr, J. Mater. Res. **7**, 1564 (1992).
[13] D. Tabor, *The Hardness of Metals* (Clarendon, Oxford, 1951).
[14] R. B. King Int. J. Solids Struct. **23**, 1657 (1987).
[15] A. V. Panin, A. R. Shugurov, and K. V. Oskomov, Phys. Solid State **47**, 2055 (2005).
[16] H. E. Boyer, *Hardness Testing* (ASM International, Metals Park, OH, 1987).
[17] A. M. Korsunsky, M. R. McGurk, S. J. Bull, and T. F. Page, Surf. Coat. Technol. **99**, 171 (1998).
[18] R. Venkatraman and J. C. Bravman, J. Mater. Res. **7**, 2040 (1992).
[19] W. D. Nix, Mater. Sci. Eng., A **37**, 234 (1997).
[20] W. D. Nix, Metall. Trans. A **20A**, 2217 (1989).
[21] C. V. Thompson, J. Mater. Res. **8**, 237 (1993).